

Article

Numerical Simulation of the Maneuvering Motion Wake of an Underwater Vehicle in Stratified Fluid

Chang Shi ^{1,2}, Xide Cheng ^{1,2,*}, Zuyuan Liu ^{1,2,*}, Kunyu Han ^{1,2}, Penghui Liu ^{1,2} and Long Jiang ^{1,2}

¹ Key Laboratory of High Performance Ship Technology, Ministry of Education, Wuhan University of Technology, Wuhan 430062, China

² School of Naval Architecture, Ocean and Energy Power Engineering, Wuhan University of Technology, Wuhan 430062, China

* Correspondence: xdccheng@whut.edu.cn (X.C.); wtulzy@whut.edu.cn (Z.L.)

Abstract: When a vehicle moves underwater, disturbance is generated and a wake remains that destroys the original free surface and produces a new wake. In order to study the mechanism and characteristics of the wave-making wake generated by the maneuvering motion of an underwater vehicle in density-stratified fluid, the k - ϵ model and the VOF method that is based on the RANS equation were used in this paper to analyze the SUBOFF model in stratified fluid at different drift angles. Numerical simulation of the maneuvering motion was carried out under these angles, and the corresponding changes in flow field caused by this motion were analyzed. The results from the comparison and analysis of the surface wave wakes under different drift angles in stratified fluid show that with the increasing drift angle, the motion wake of the vehicle still exhibits obvious Kelvin wave system characteristics. However, there are significant changes in hydrodynamic performance. The asymmetry of the surrounding flow field will increase with the increase in the drift angle. The pressure of the underwater vehicle is inversely proportional to the velocity of the surrounding flow field, and the amplitude of the peak and trough of the free surface wave is linearly related to the change in the drift angle. The numerical simulation can serve as a reference for the non-acoustic detection of the motion heading of an underwater vehicle and the motion trajectory of anti-reconnaissance underwater vehicles under actual sea conditions.



Citation: Shi, C.; Cheng, X.; Liu, Z.; Han, K.; Liu, P.; Jiang, L. Numerical Simulation of the Maneuvering Motion Wake of an Underwater Vehicle in Stratified Fluid. *J. Mar. Sci. Eng.* **2022**, *10*, 1672. <https://doi.org/10.3390/jmse10111672>

Academic Editor: María Isabel Lamas Galdo

Received: 14 October 2022

Accepted: 30 October 2022

Published: 6 November 2022

Publisher's Note: MDPI stays neutral with regard to jurisdictional claims in published maps and institutional affiliations.



Copyright: © 2022 by the authors. Licensee MDPI, Basel, Switzerland. This article is an open access article distributed under the terms and conditions of the Creative Commons Attribution (CC BY) license (<https://creativecommons.org/licenses/by/4.0/>).

1. Introduction

Enhancing naval power is crucial to ensuring the security of a country's territorial waters. An important research topic in modern warfare is how to improve the concealment of underwater vehicles. With the rapid development of materials and manufacturing technology, the navigation noise of underwater vehicles has been greatly reduced and can even be masked by the natural noise in oceans. Therefore, the non-acoustic detection of underwater vehicles has gradually become a research hotspot. Results from research into how to reduce the physical flow field and wake on the water surface are providing new ideas for the anti-submarine design of underwater vehicles.

Scientific research has shown that seawater in various regions of Earth presents a regular macro-level structure in terms of vertical distribution. Generally speaking, the temperature of seawater decreases with increasing depth, and the density increases with increasing depth [1]. Underwater vehicles sail in stratified fluid, resulting in the generation of internal waves, which increase the sailing resistance of the ship. During an expedition, Nansen et al. [2] found that when a ship passed through the Arctic Ocean region, its speed decreased significantly while its resistance increased; this phenomenon was dubbed "dead water". In 1963, an American submarine was swept under the sea by internal ocean waves. The submarine was overloaded, which was responsible for this tragedy, in which no one survived [3]. After this incident, stratified fluid received great attention in

research. Allen H et al. [4] showed that the wake of vehicle motion in stratified fluid is very different from that in uniform flow. Hopfinger et al. [5] used fluorescent dye technology to study the gravitational waves and wakes of balls moving in stratified fluids. Chomaz et al. [6] presented experimental results of the structure of the wake of spheres moving in uniform and stratified fluids. The results show that a wake has two characteristic frequencies in homogeneous fluids. These two eigenfrequencies correspond to the two distinct unstable modes, namely the Kelvin–Helmholtz instability mode and the spiral instability mode. Huiyang Ma et al. [7] studied the interaction of moving objects in stratified fluid through experiments and numerical simulations of a Rankine submarine, focusing on the effect of the speed and shape of moving objects on the free surface. Jianming Jin et al. [8,9] carried out numerical simulation of small spheres in stratified fluid, analyzing and studying the resulting motion wake and successfully simulating the internal and the surface waves generated by the motion of a small ball in a stratified fluid. Yu Chang et al. [10] used the numerical simulation method of CFD to simulate the wake produced by the movement of the SUBOFF standard mode in stratified fluid. Brucker et al. [11] compared the characteristic velocity and length scales of self-propelled wakes and trailing wakes in stratified fluid, representing the beginning of analyses into self-propelled wake characteristics. James W et al. [12] used large eddy simulations to study the full-scale wake of a submarine. He calculated the motion wakes of elongated bodies both in homogeneous and in stratified fluids. Amin A et al. [13] studied the wake and internal waves of a moving three-dimensional airfoil body in a layered fluid by using the method of a flow field shadow map in a layered water tank with limited depth. Moody et al. [14] used a combination of numerical simulations, field measurements, and laboratory experiments to study the wake produced by submerged propagating bodies in stratified fluid. Qingjie Meng et al. [15] carried out numerical simulation of a SUBOFF model in uniform fluid and stratified fluid. Analyzing the trails produced by the contrast. Weizhuang Ma et al. [16,17] used a two-layer model to simulate stratified flow with a clamshell. The near-field flow of a real-scale submarine in stratified flow was simulated using a proposed method, in which they analyzed the effects of stratified flow, the diving depth of the submarine, and the speed of the submarine on free surface waves and internal wave characteristics. This led to the proposal of a new numerical simulation method to achieve continuous density stratification in temperature-dominated regimes. Wei Lu et al. [18] studied the variation of drag coefficient of a SUBOFF submarine sailing in different Froude numbers and the influence of internal wave interfaces on wave-making in a stratified marine environment. Qianqian Zhang et al. [19,20] calculated the resistance value of a box structure in stratified fluid, exploring the characteristics and changes in structural resistance, resistance changes, and wake changes for SUBOFFs navigating in stratified fluid. Jianwei Wu et al. [21] studied the characteristics of free surface wake caused by the motion of a fully attached SUBOFF submarine at different diving depths in a continuous density gradient environment. Liu Shuang et al. [22–26] studied the resistance and flow field of a SUBOFF at different forward speeds, submerged positions, and fluid density changes in addition to the influence of self-propulsion of submarines with different attachments on the surface waves and internal waves. Studies have shown that the forward speed and diving depth of a submarine significantly impact on its hydrodynamic performance, whereby the density of the bottom layer and the distance of the submarine from the inner surface have little effect. The effect of stratified fluid on drag increases with advancing speed and for positions closer to the free surface. The internal waves of a submarine navigating below the internal interface are significantly different from those of a submarine navigating above the internal interface. Cao et al. [27–29] proposed a method for predicting density-stratified fluid wakes involving navigation of the Joubert BB2 model in uniform and linear stratified fluids for numerical simulations. Resistance, internal waves, and surface characteristics were compared, with discussion of the characteristics of stratified fluid properties.

At present, most studies have mainly considered the wake induced by the straight motion of an underwater vehicle in stratified fluid, and the wake caused by the maneu-

vering motion of the underwater vehicle in stratified fluid has received little attention. In view of the special sea conditions of stratified fluid, it is essential to analyze the wake changes caused by the maneuvering motion of an underwater vehicle according to variable drift angles.

In this study, a computational fluid dynamics method was used to carry out numerical simulations for analyzing the surface wave wake changes caused by underwater vehicles. The numerical simulation model of density stratified flow was established using CFD (computational fluid dynamics). First, the numerical model was verified to ensure the accuracy and rationality of the method. The fully attached SUBOFF submarine was then used as the basic model for research, and the navigation under different conditions was carried out at certain speeds. The hydrodynamic characteristics and wake characteristics of SUBOFF after variable drift angle maneuvering in stratified fluid were then analyzed.

2. Numerical Method and Model

2.1. Governing Equations

Based on the RANS (Reynolds-averaged Navier-Stokes) equations, the incompressible flow governing equation is:

$$\frac{\partial U_i}{\partial x_i} = 0 \quad (1)$$

$$\rho \frac{\partial \bar{u}_i}{\partial t} + \rho \partial \bar{u}_j \frac{\partial \bar{u}_i}{\partial x_j} = \rho \bar{F}_i - \frac{\partial \bar{p}}{\partial x_i} + \frac{\partial}{\partial x_j} \left(\mu \frac{\partial \bar{u}_i}{\partial x_j} - \rho \bar{u}'_i \bar{u}'_j \right) \quad (2)$$

where \bar{u}_i and u'_i are the Reynolds average velocity and pulsation velocity; $\rho u'_i u'_j$ is the Reynolds stress term; \bar{F}_i is the mass force; ρ is the fluid density. Equation (1) is the continuity equation, and Equation (2) is the momentum equation.

2.2. Turbulence Model

The calculation uses the standard $k-\varepsilon$ turbulence model to resolve the governing equations. The transport equation of k and ε in incompressible flow is:

$$\frac{\partial(\rho k)}{\partial t} + \frac{\partial(\rho k u_i)}{\partial x_i} = \frac{\partial}{\partial x_j} \left[\left(\mu + \frac{\mu_t}{\sigma_k} \right) \frac{\partial k}{\partial x_j} \right] + G_k - \rho \varepsilon + S_k \quad (3)$$

$$\frac{\partial(\rho \varepsilon)}{\partial t} + \frac{\partial(\rho \varepsilon u_i)}{\partial x_i} = \frac{\partial}{\partial x_j} \left[\left(\mu + \frac{\mu_t}{\sigma_\varepsilon} \right) \frac{\partial \varepsilon}{\partial x_j} \right] + G_{1\varepsilon} \frac{\varepsilon}{k} G_k - G_{2\varepsilon} \rho \frac{\varepsilon^2}{k} + S_\varepsilon \quad (4)$$

In the formula, the turbulent viscosity $\mu_t = \rho C_\mu \frac{k^2}{\varepsilon}$, the generation term of the turbulent kinetic energy k caused by the average velocity gradient $G_k = -\rho \bar{u}_i \bar{u}_j \frac{\partial u_i}{\partial x_j}$, and S_k are S_k user-defined source items.

2.3. VOF Equation

The VOF (volume of fluid) method realizes the tracking of the evolution of the free surface by the volume fraction of the grid cells occupied by the fluid. In this method, all fluids satisfy the same momentum equation. The location of the interface is determined by tracking the volume fraction of each fluid in the computational unit over the entire computational area.

Assuming that the volume fraction of the q -th fluid in the cell is, for the q -th fluid:

$$\frac{\partial \alpha_q}{\partial t} + u_i \frac{\partial \alpha_q}{\partial x_i} = 0 \quad (5)$$

The sum of the fluid volume fractions is 1. When $\alpha_q = 0$, it means that the q th phase fluid does not exist in the control unit; when $\alpha_q = 1$, it means that the q -th phase fluid is

filled in the control unit; when $0 < \alpha_q < 1$, it means that the qth phase fluid exists in the control unit between q phase fluids and other fluids.

3. Numerical Modeling and Validation

3.1. Verification of Computational Model Reliability

There are few studies on the resistance and wave-building characteristics of underwater vehicles in stratified flow. The research in this paper is based on STAR-CCM+ software for simulation. First, the numerical model was verified, and the modeling was carried out according to the parameters of the experimental device in the literature [19,20]. As shown in Figure 1, the depth of the pool is 0.6 m. Fresh water is distributed in the upper layer. The density is $\rho_1 = 997.561 \text{ kg/m}^3$. The lower layer is salt water. The density $\rho_2 = 1024 \text{ kg/m}^3$. The thickness of the lower layer is 0.3 m. The experimental model is a box-shaped structure with a length, width, and height of 0.6, 0.45, and 0.35 m, respectively. The box-shaped structure has a draft of 0.2 m and trailer speeds of 0.14, 0.16, 0.18, 0.20 and 0.24 m/s. The towing resistance calculation model verified by this numerical value is completely consistent with the experimental model.

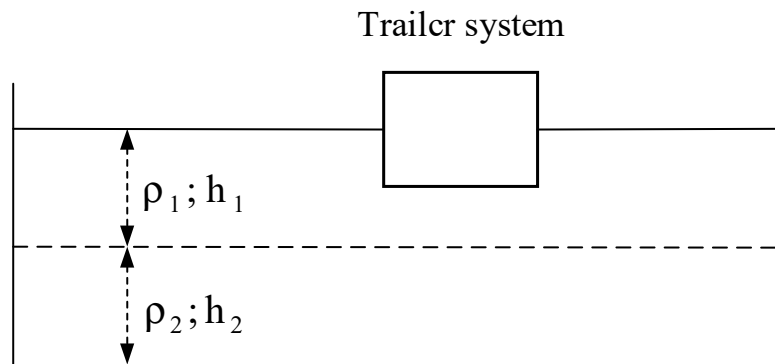


Figure 1. Experimental diagram for towing resistance of box structure.

In this paper, a numerical simulation method was used to calculate the resistance of box-shaped structures in stratified fluid under different traction velocities. The resistance values from analytical experiments and numerical simulations in the literature were compared [26] as shown in Figure 2. It can be seen from the figure that the numerical simulation results are in good agreement with the experimental results and the CFD simulation results. Table 1 shows the experimental results for resistance of the box-shaped structure in the traction test, the CFD resistance calculation results of other reports, and the CFD resistance calculation results of this paper. $\text{Error} = \left| \frac{R_{\text{CFD}} - R_{\text{Exp}}}{R_{\text{Exp}}} \right|$. Therefore, from the results in Figure 2 and Table 1, it can be concluded that the numerical method in this paper can more accurately calculate the hydrodynamic performance of underwater vehicles in stratified fluids.

Table 1. The experimental results for resistance of the box-shaped structure.

Velocity/(m/s)	Experiment/(N)	Literature/(N)	CFD/(N)	Error/(\%)
0.06	0.238	0.238	0.289	17.60%
0.08	0.558	0.414	0.619	10.90%
0.1	1.072	0.806	1.01	5.78%
0.12	1.495	1.248	1.429	4.41%
0.14	1.888	1.675	1.816	3.81%
0.16	2.136	2.136	2.136	0
0.18	2.384	2.491	2.399	0.63%
0.2	2.722	2.567	2.655	2.46%
0.24	3.36	3.146	3.22	4.17%

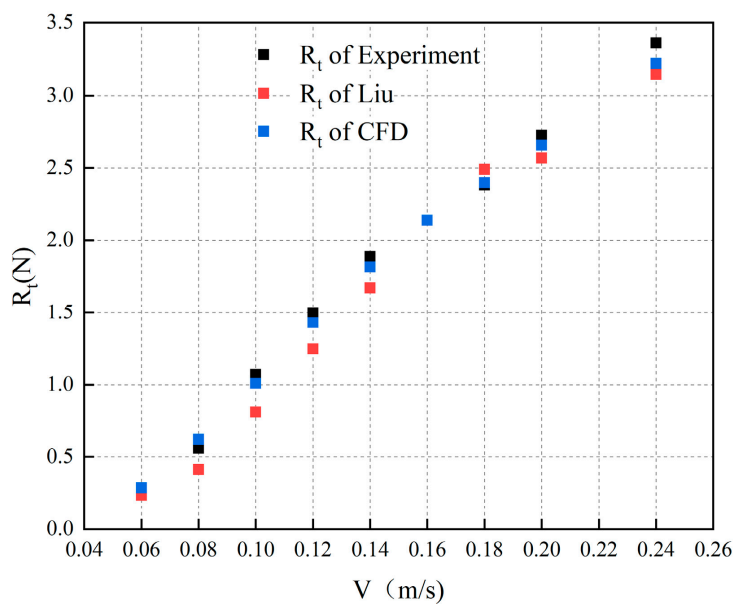


Figure 2. Comparison of numerical simulation results.

Secondly, the SUBOFF bare hull in the numerical simulation literature [26] is in a direct sailing condition in a layered environment. The calculation model is shown in Figure 3. The length of the bare hull is 99.4 m. The upper fluid is fresh water. The density $\rho_1 = 997.561 \text{ kg/m}^3$. The lower fluid is salt water. $\rho_2 = 1024 \text{ kg/m}^3$. $D_1 = 0.16 \text{ L}$. $d_2 = 0.1 \text{ L}$. The sailing speed is $\text{Fr} = 0.5$.

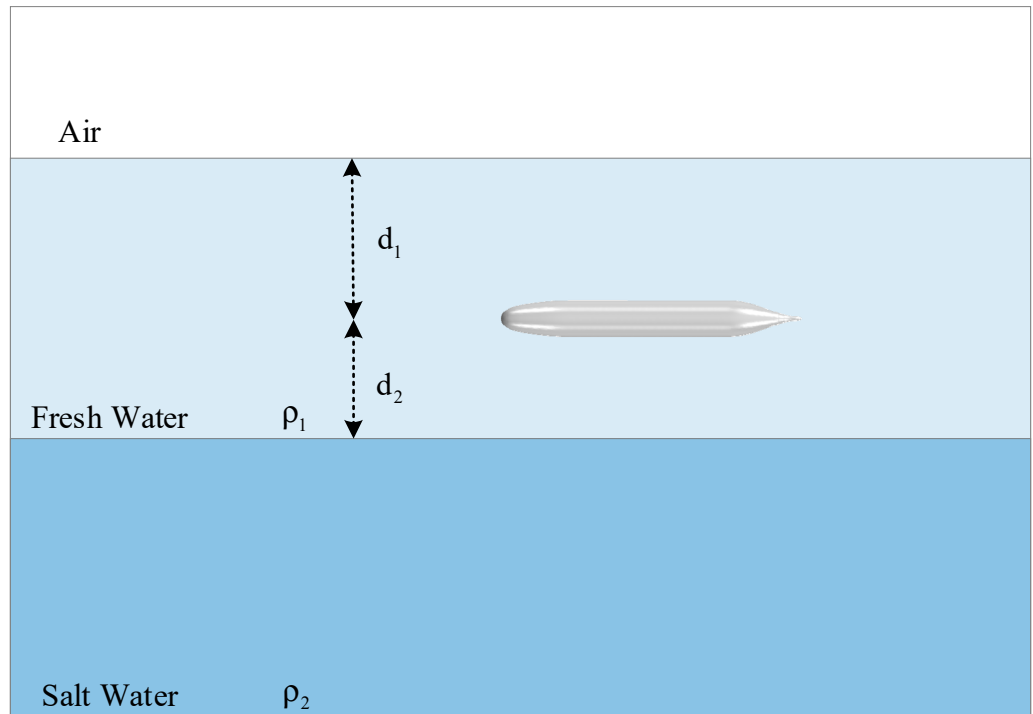


Figure 3. Model diagram.

Under this condition, the first period wavelength of the free surface wake in the literature is 1.288 times that of the model. This article used the SUBOFF bareboat standard model. The longitudinal section wave shear diagram was obtained by simulating the literature conditions. The wavelength of the first period of the free liquid surface in Figure 4

is 5.6 m, and the wavelength is 1.286 times that of the calculation model. The calculated wavelengths were compared with wavelength multiples in the literature, and the error is 0.152%. Overall, the CFD calculation results show good agreement with the literature results. The results show that the model in this paper has a good simulation effect on wave-making wakes.

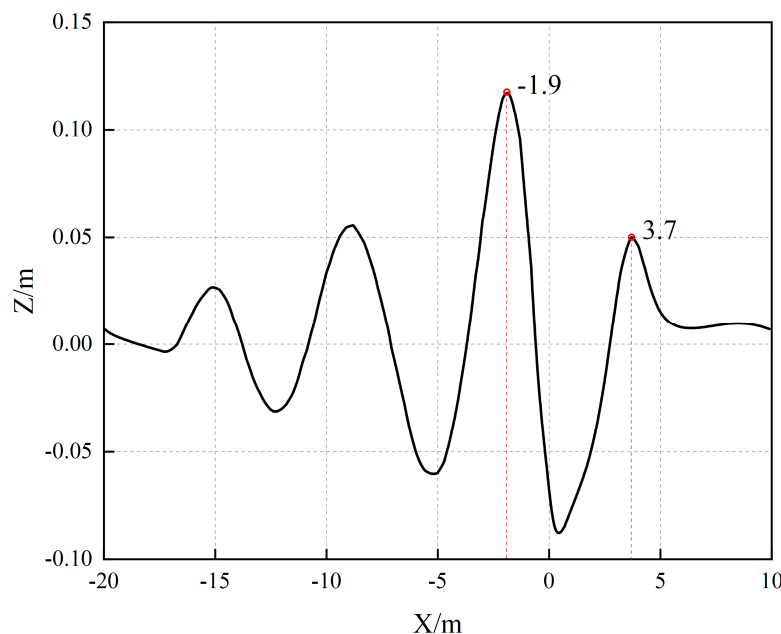


Figure 4. Longitudinal section wave cut diagram of direct flight.

3.2. Numerical Simulation Related Settings

This paper adopted the standard SUBOFF model with full attachment as the calculation object. The model is shown in Figure 5. Table 2 is the main element table of the fully attached SUBOFF.



Figure 5. Full-body SUBOFF geometric model.

Table 2. Table of main elements of fully attached SUBOFF.

Parameters	Size/m
L	4.356
Maximum hull diameter	0.254
Length between vertical lines	4.261
Longitudinal position of floating center	$0.4612L_{\text{oa}}$

The computational domain settings are shown in Figure 6, which were set to prevent backflow in the numerical simulation from affecting the calculation results. In this paper, the dimensions are two times the captain's length in front of the boat, 10 times the captain's length at the rear of the boat, 5 times the captain's length on the side of the boat, and 1 times the captain's length from the hull to the bottom of the calculation domain for performing wave elimination processing. The surface boundary condition type of the vehicle is a wall, and the object surface condition is no-slip. The Euler multiphase flow method was used with customization of the volume fraction and density of the liquid. The pressure is based

on density. The inlet boundary condition type is a velocity inlet, and the outlet boundary condition is a pressure outlet.

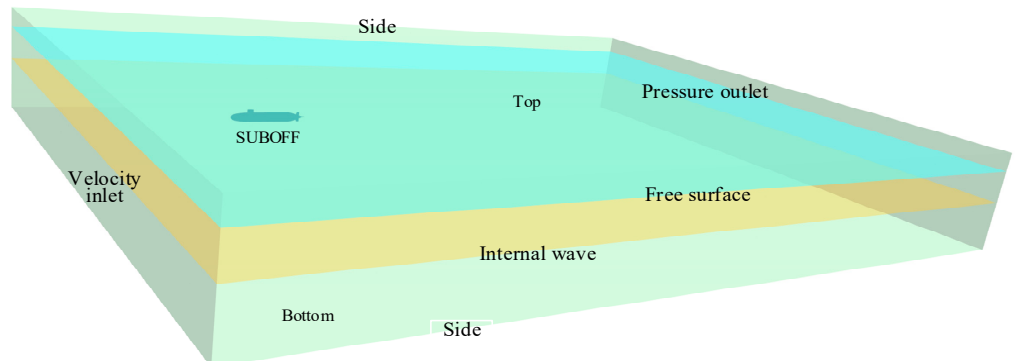


Figure 6. Computational domain and hull boundary conditions.

The density layer interface and the surface wave interface were encrypted to ensure that the navigation characteristics of the navigation body in layered fluid could be accurately captured. The hull of the sailing body and the appendages of the sailing body were densified, and the boundary meshes were processed by the cutting body mesh and the prism layer mesh generator. The grid distribution around the vehicle is shown in Figure 7.

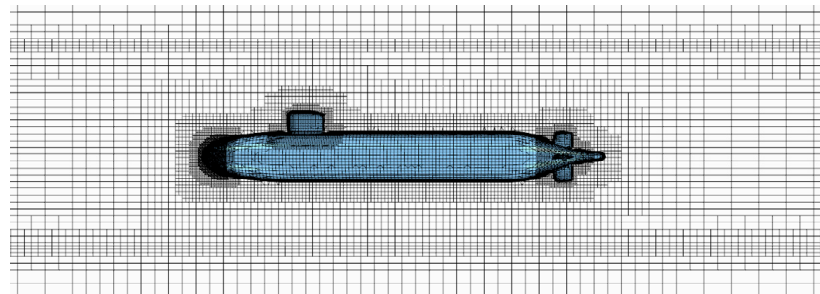


Figure 7. Computational domain meshing.

In the computational domain, the fluid density changes vertically, and the stratification phenomenon is shown in Figure 8. SUBOFF sails in the upper freshwater layer at different drift angles. The diving depth is $h_1 = 1.2$ m. The distance from the center of gravity of the voyage to the freshwater–saltwater boundary layer is $h_2 = 1.0$ m. ρ_1 , ρ_2 are the fluid densities of freshwater and saline aquifers, respectively, $\rho_1 = 997.561$ kg/m³, $\rho_2 = 1024$ kg/m³.

3.3. Convergence Verification

In this paper, the convergence of the SUBOFF vehicle in the direct flight condition was verified. The test conditions made by Roddy [30] in 1990 were used. Here, a fixed speed of 11.85 kn was selected, and three groups of different grid sizes were selected for grid convergence research. The grid numbers are 2.23 million, 5.33 million, and 7.12 million, respectively, and a computation time step of 0.01 s was selected. Table 2 shows the influence on the total resistance calculation results when the number of grids is changed. It can be seen from Table 3 that when the number of grids is 5.33 million, the error is 0.44%. The calculation results show little effect, indicating that the mesh is converged. Considering the computing resources, a grid model of 5.33 million was used for calculation.

$$\text{Error}_i = \left| \frac{R_i - R_A}{R_A} \right|, i = A, B, C$$

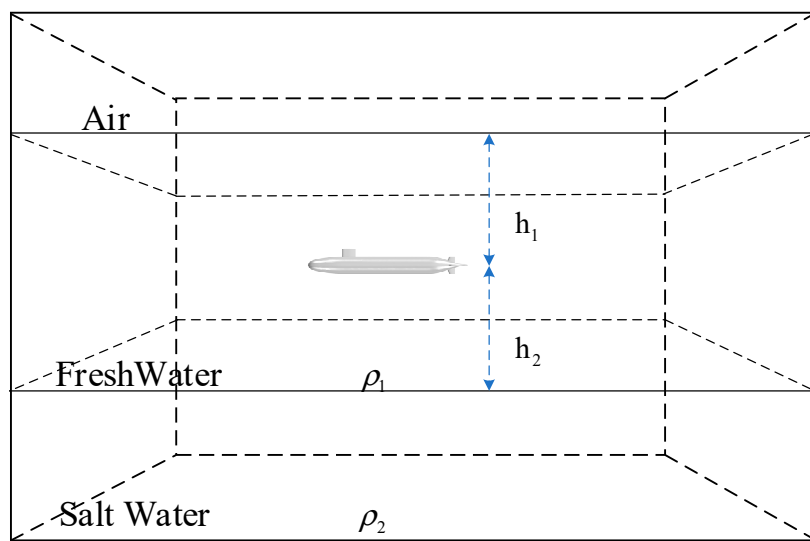


Figure 8. Schematic diagram of fluid density stratification.

Table 3. Mesh convergence verification.

Mesh	Amount	Rt/N	Error
A	7.12 M	412.72	0
B	5.33 M	414.55	0.44%
C	2.23 M	439.87	6.17%

Meanwhile, three different time-stepping schemes were employed to verify the time-step-independent verification. At this time, a mesh model with a mesh number of 5.33 million was used. The time steps of 0.005, 0.01, and 0.045 s were taken for verification. The results are shown in Table 4. It can be seen that the time step is reduced from 0.01 to 0.005 s, and the resistance error is 0.25%. The error of the total resistance is small, indicating that the change in the time step has little effect on the calculation results. Therefore, a time step of 0.01 s was used for subsequent calculations.

Table 4. Time step convergence.

Time	Time Step/s	Rt/N	Error
A	0.005	413.51	0
B	0.01	414.55	0.25%
C	0.045	416.42	0.70%

4. Maneuvering Kinematic Characteristics of Underwater Vehicle in Stratified Fluid

4.1. Speed Distribution

In order to study the influence of different drift angles on the maneuvering characteristics of the vehicle, this paper numerically simulated the navigation conditions of SUBOFF with different drift angles in a layered environment. The direction of the sailing speed of the vehicle is always in the positive direction of the X-axis. Here, the positive X direction is the direction of the vehicle from the tail to the head. In Figure 9, SUBOFF deflects in the positive direction of the Y-axis with the center of mass as the origin. Figure 9 is a velocity diagram of the vehicle cross section when the velocity of SUBOFF is 11.83 kn. It shows the cross-sectional velocity diagram for drift angles of 2°, 4°, 6°, 8°, 10° and 12°. The results in the figure show that the larger the drift angle, the more severe the asymmetry of the speed. The closer the lowest point of the front speed of the boat is to the side of the boat, the greater the directional deviation of the tail speed. As the drift angle increases, the bow speed on the positive side of the Y-axis increases. The speed at the front of the rudder becomes

increasingly smaller. On the contrary, the forward speed of the boat on the negative side of the Y-axis gradually decreases, whereas the speed at the front of the rudder increases. At the same time, this also shows that a change in the drift angle can cause changes in the hull pressure and flow field.

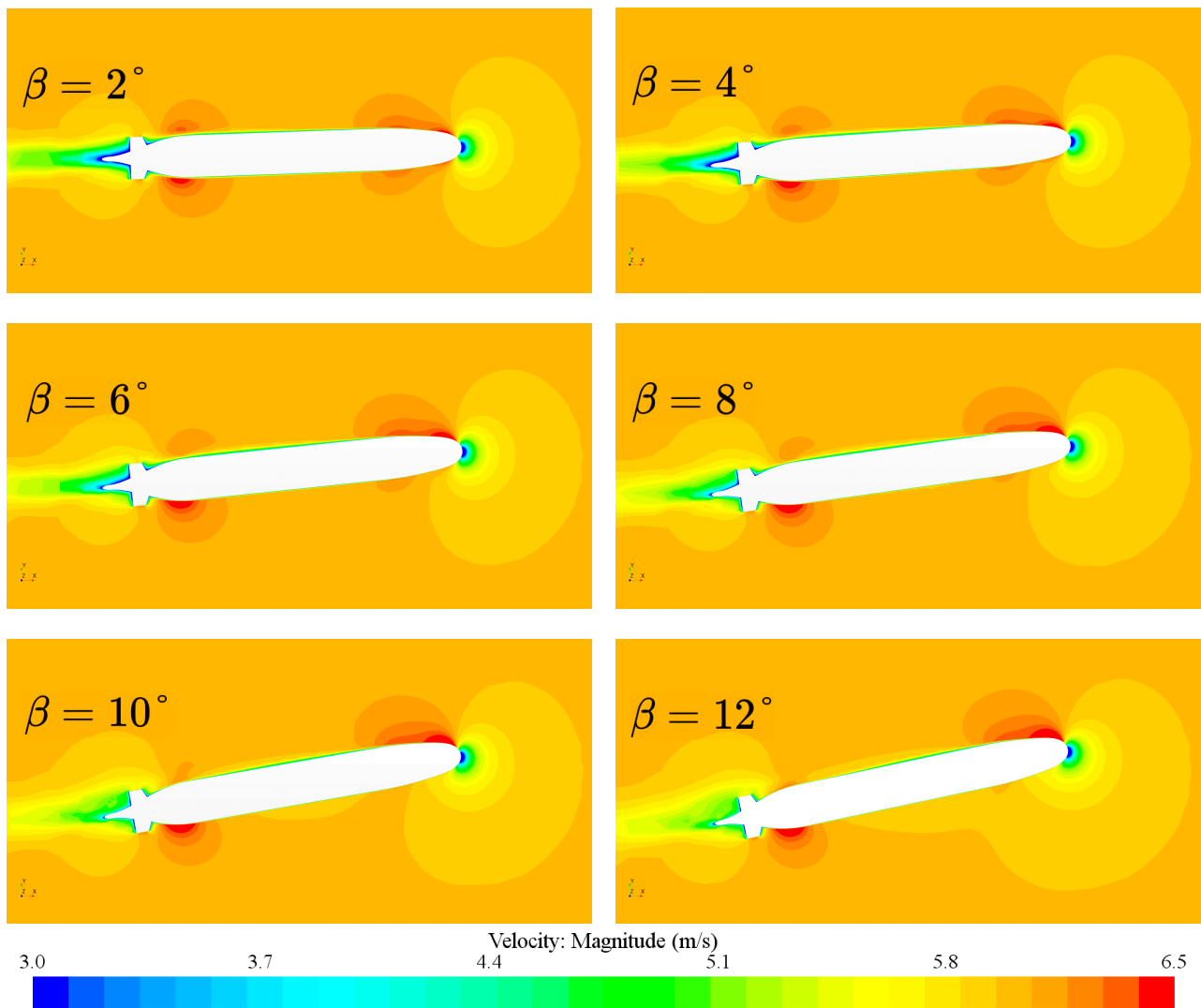


Figure 9. Comparison diagram of velocity field around different drift angle.

4.2. Pressure Distribution

The changes of the SUBOFF sailing characteristics under the condition of variable drift angle were further studied. In this paper, the distribution of the SUBOFF cross-sectional pressure along the length of the boat and the surface pressure were calculated and compared. Figure 10 shows the pressure distribution on both sides of the Y-axis of the SUBOFF cross section at drift angles of 2° , 4° , 6° , 8° , 10° , and 12° . The direction of the hull is in the positive direction of the X-axis. It can be seen from the calculation results in Figure 8 that there are two peaks in the SUBOFF cross-sectional pressure, which correspond to pressure on either the bow part or the rudder part of the boat. The pressure mutation has higher requirements for the intensity of the corresponding position. At the same time, the sudden change in pressure also accordingly changes the state of the flow field at this location. This situation is not conducive to vehicle concealment. With increases in drift angle, the pressure difference on both sides of the hull also increases. The larger the drift angle, the smaller the bow pressure on the positive side of the Y-axis and the greater the

pressure on the tail rudder part. Conversely, when the pressure on the bow on the negative side of the Y-axis increases, the pressure on the rudder part decreases, and the pressure difference on both sides of the hull also increases.

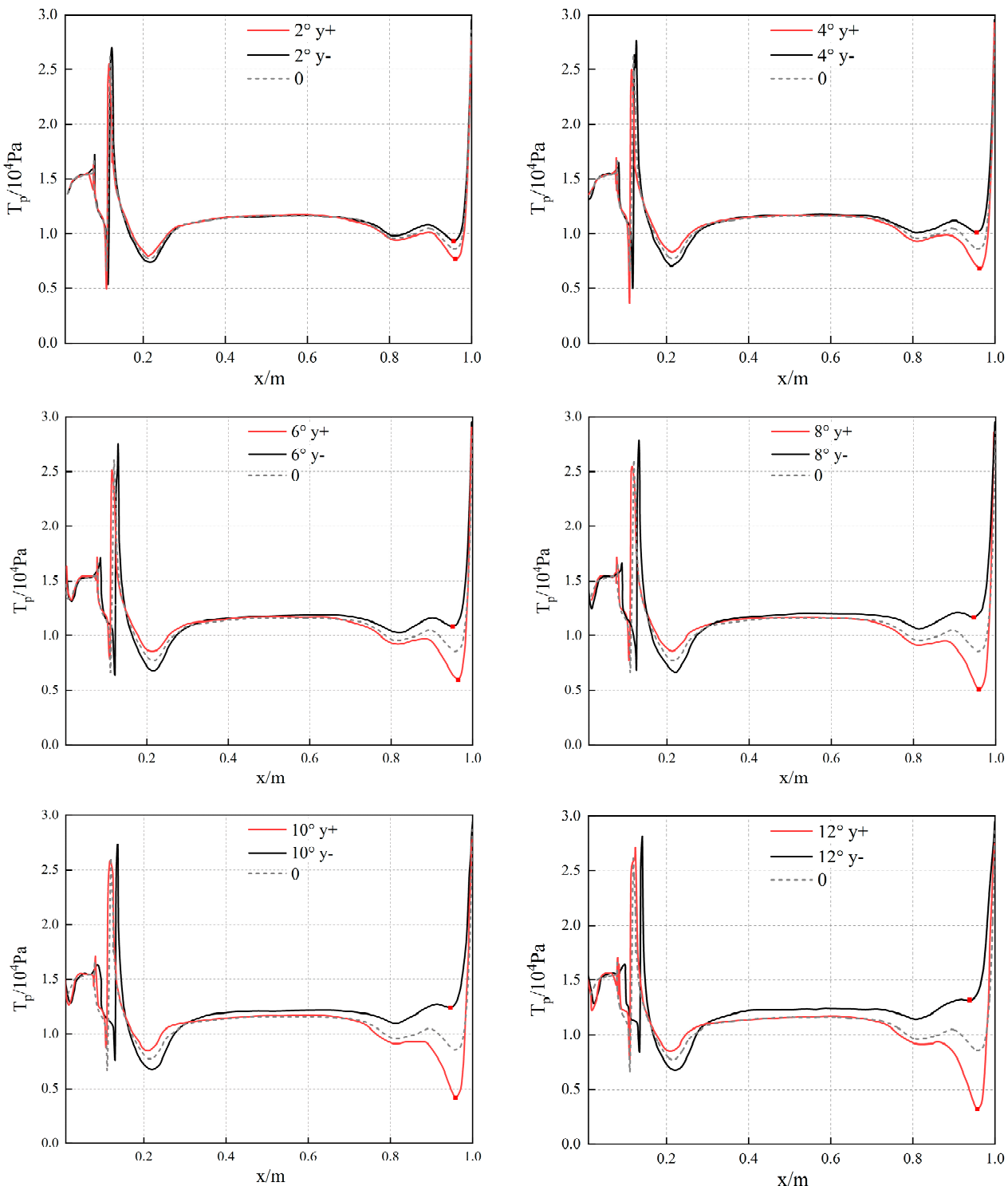


Figure 10. Comparison of body pressure at different drift angles.

It can be seen from Figures 9 and 10 that the pressure on the bow of SUBOFF is high, and the velocity of the flow field around the bow is significantly reduced. The pressure on the bow part on one side of the positive direction of the Y-axis gradually decreases. The smoothing speed around this part is significantly increased. The pressure on the bow part

of one side in the negative direction of the Y-axis decreases with an increasing drift angle. In contrast, the velocity of the flow field around this part is significantly reduced. Wake fluctuations can also have a significant impact.

The point with the largest pressure difference between the left and right sides of the hull is marked in red in Figure 10. Table 5 shows the pressure value at the red mark, and Figure 11 is the numerical graph of the pressure value at the red point. It can be seen from Table 5 and Figure 11 that with the increase in the drift angle, the pressure in the negative direction of the Y-axis at the red mark gradually increases and has a linear relationship with a linear function; meanwhile, the pressure in the positive direction of the Y-axis at the red mark decreases gradually, also showing the linear relationship of a linear function. It can be determined from this that when the underwater vehicle performs a maneuvering movement with variable drift angle, the pressure difference of the two sides of the hull increases and then decreases. By adding up the pressure at the marks on both sides of different drift angles, it can be seen that the sum of the pressures on both sides of the hull at different drift angles remains unchanged. In performing the calculation with the first set of pressure sums results, it was observed that the error is less than 4%.

$$\text{Error}_i = \left| \frac{(T_p(y-) + T_p(y-))_{2^\circ} - (T_p(y-) + T_p(y-))_{i^\circ}}{(T_p(y-) + T_p(y-))_{2^\circ}} \right|, i = 2, 4, 6, 8, 10, 12$$

Table 5. Pressure gauge at the red mark.

Drift Angle β	$T_p(y-)/10^4 \text{ Pa}$	$T_p(y+)/10^4 \text{ Pa}$	$T_p(y-)+T_p(y+)/10^4 \text{ Pa}$	Error
2°	0.93	0.766	1.696	0
4°	1.01	0.685	1.695	0.14%
6°	1.085	0.6	1.685	0.65%
8°	1.164	0.507	1.671	1.47%
10°	1.243	0.418	1.661	2.06%
12°	1.312	0.322	1.634	3.66%

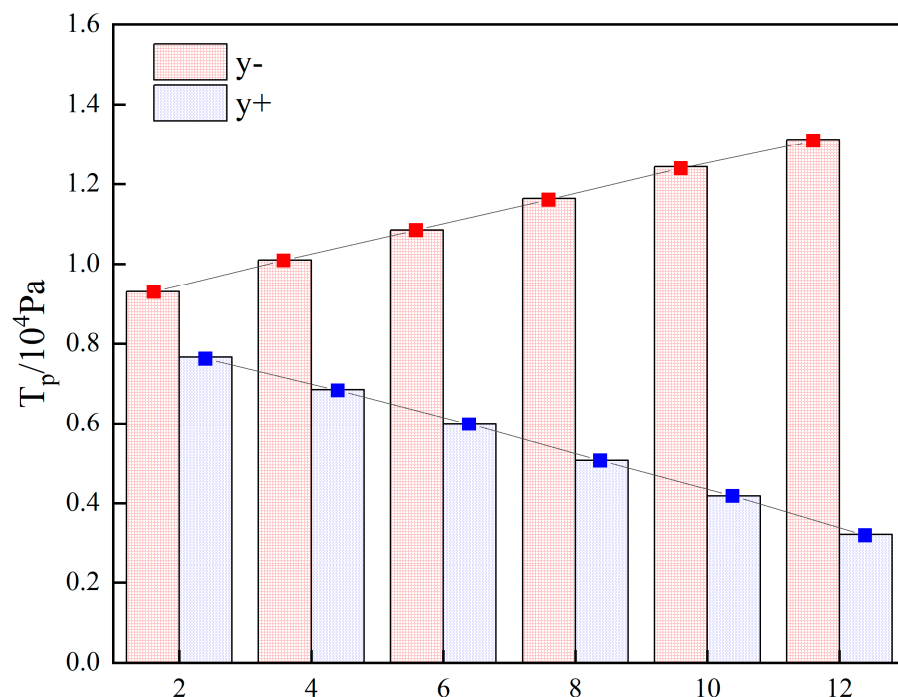


Figure 11. Pressure map comparison at the red mark.

4.3. Wake Feature

In this paper, the characteristics of the free surface of the SUBOFF wake under different drift angle conditions were calculated, analyzed, and compared. Figure 12 is a comparison chart of the calculation results of the SUBOFF wake feature at drift angles of 2° , 4° , 6° , 8° , 10° , and 12° . The results show that the wakes generated by SUBOFF under different working conditions all exhibit significant Kelvin wave system characteristics. Due to the higher vehicle speed, the scattered wave characteristics in the wake are more obvious than the shear wave characteristics. The asymmetry of the wake in the free surface is also more pronounced, and the concealment of the vehicular body is weakened. As the drift angle increases, the amplitude of the scattered wave on the positive side of the Y-axis decreases. The amplitude of the scattered wave increases in the negative direction of the Y-axis.

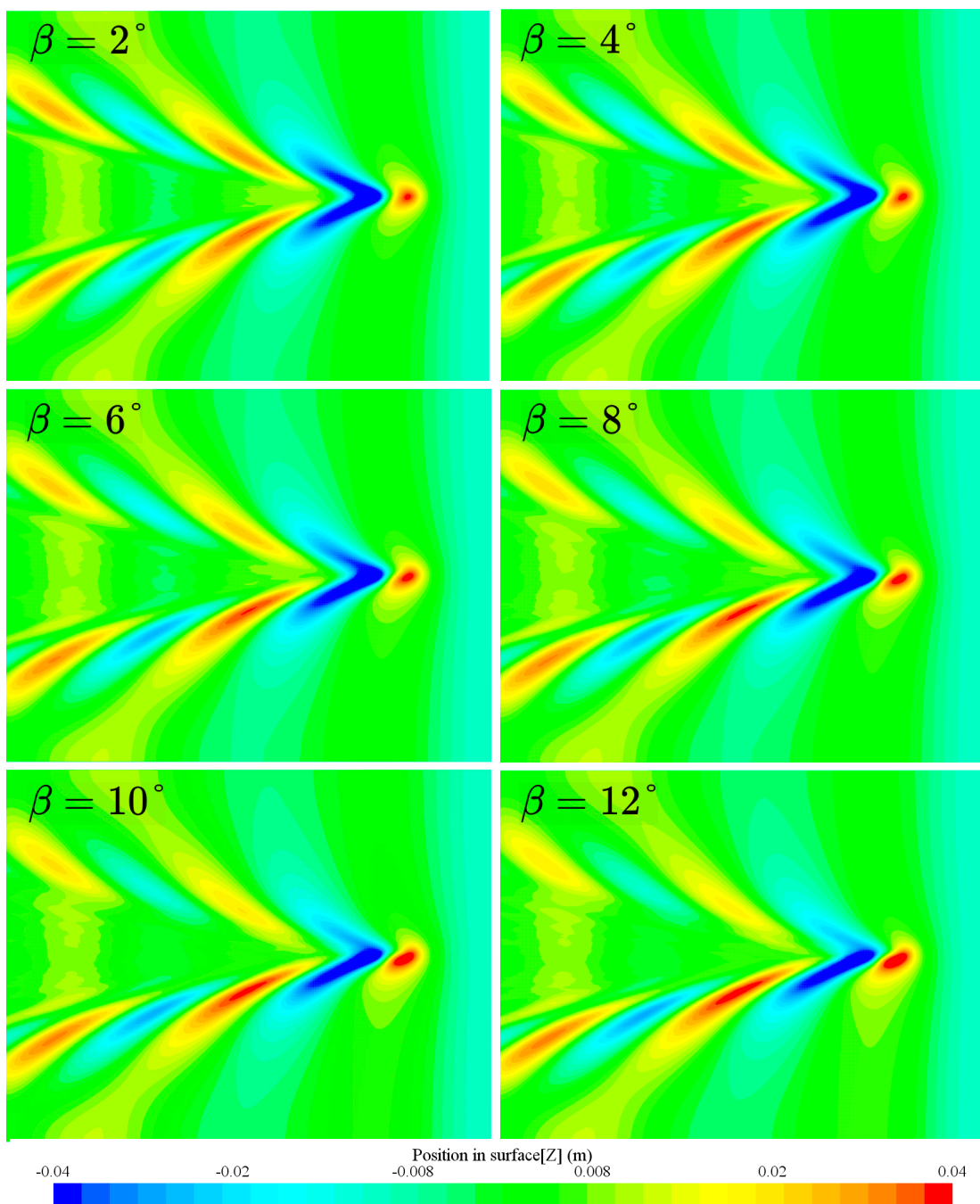


Figure 12. Free surface wave wake at different drift angle.

Figure 13 is the wave shear diagram of the longitudinal section of the free surface under different drift angle conditions. It can be seen from the figure that under different drift angles, the amplitude changes are quite varied, and the wavelength does not change. It can be concluded that when the underwater vehicle moves in stratified fluid, the drift angle change does not affect the wake wavelength of the underwater vehicle.

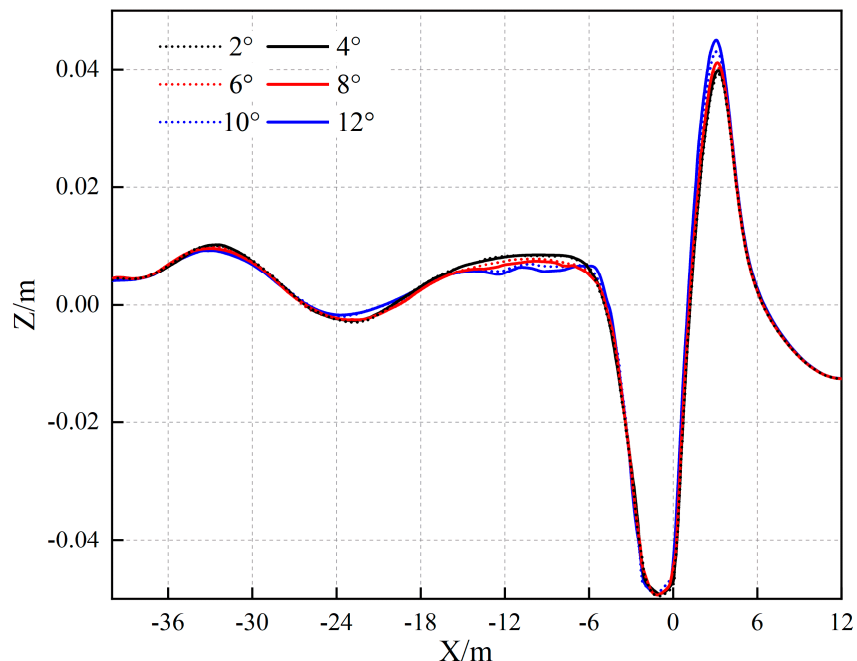


Figure 13. Comparison of the longitudinal profile wave cut diagram with different drift angles.

Figure 14 is a longitudinal wave cut diagram obtained at different X positions, where the ordinate is the wave front lift Z. The abscissa is the dimension unit in the Y direction, and the unit is m. Starting from the bow ($X = 0$), a transverse wave tangent was obtained for every other length of the boat, and Figure 13 was obtained. Figure ($X = 0$) is the transverse wave tangent at the bow. Figure ($X = L$) is the transverse wave shear diagram at the stern of the boat. By analogy, Figure ($X = 8 L$) is the transverse wake wave cut diagram, where the wake propagates eight times the length of the boat. It can be seen from Figure 14 that when SUBOFF navigates in a layered environment, it is propagated backwards, generating a wave. The peaks and valleys in the middle of the wave tangent continue to expand to both sides. Starting from the graph ($X = 4 L$), the fluctuations of the part of the wake near the origin of the Y-axis change. The peaks and troughs in the middle are continuously stretched, and there is no major fluctuation in amplitude. The middle waveform has smaller amplitude fluctuations. As the wave-making is propagated backwards, such small-amplitude fluctuations become increasingly frequent. At the same time, the distance between the peaks of large magnitudes gradually increases.

Combining Figures 12 and 14, it can be seen that as the drift angle increases, the height of the first wave crest from right to left increases, though the height of the trough is reduced. It can be seen from Figures 12–14 that as the drift angle increases, the crests and troughs on both sides undulate, and the asymmetry increases. It is obvious that the drift angle increases, and the fluctuation amplitude in the positive direction of the Y-axis decreases significantly. The volatility in the negative direction has increased significantly. Therefore, when the vehicle sails in a layered environment, changing the drift angle will not change the wavelength of the wake but only increase the wake asymmetry.

$$\text{Difference}_i = \left| \frac{X_{i^\circ} - X_{2^\circ}}{X_{2^\circ}} \right|, i = 2, 4, 6, 8, 10, 12$$

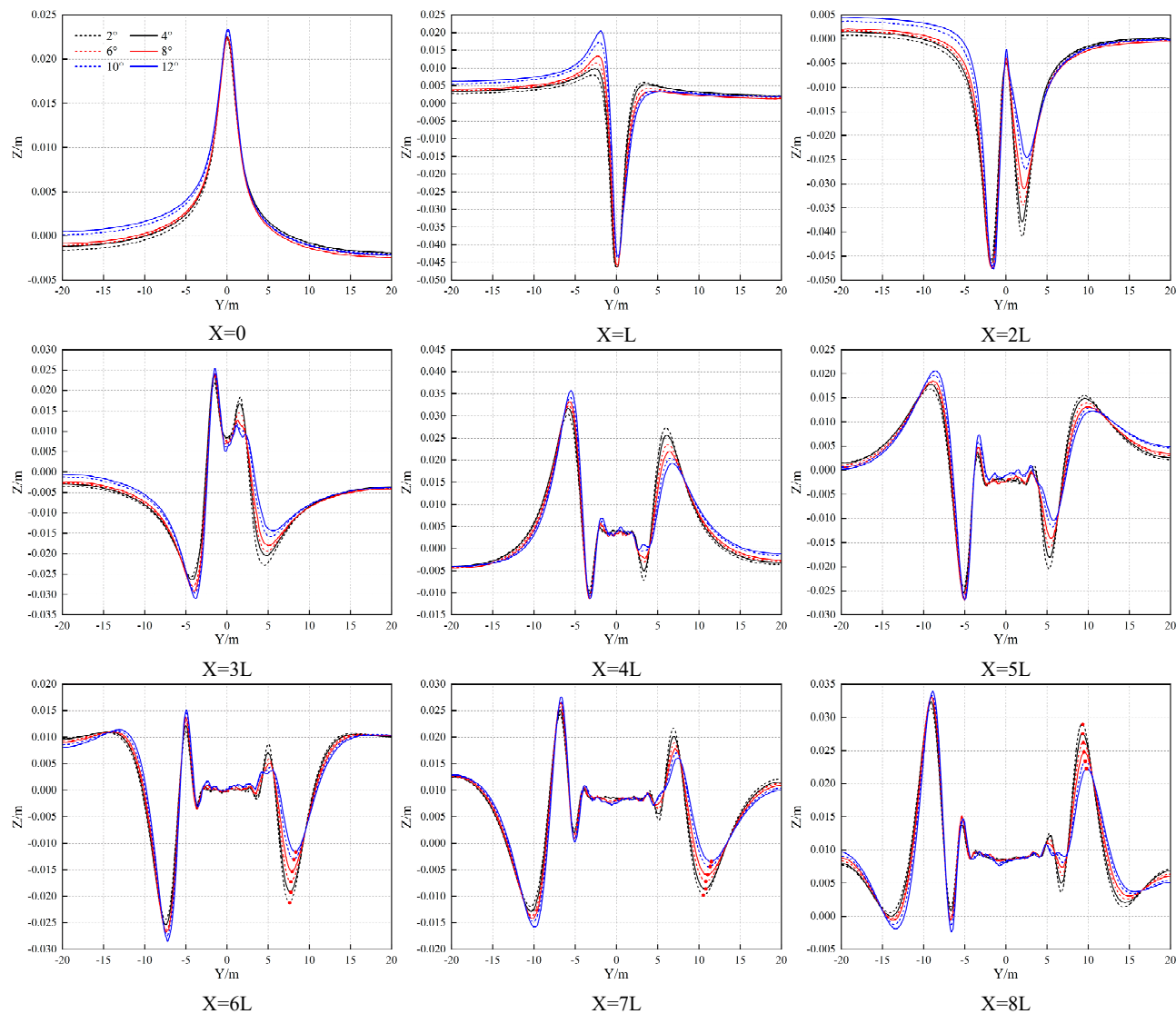


Figure 14. Comparison of transverse wave cutting at different drift angles and different positions.

Table 6 shows the values of wave crests or troughs of different drift angles of the cross-sectional wave shear diagrams of $X = 6 L$; $X = 7 L$, and $X = 8 L$ in Figure 14. The difference part of the table represents the absolute value of the increment of the wave height amplitude. It can be seen from Table 6 that the wave height amplitude almost uniformly increases.

Table 6. Wave height value table.

Drift Angle β	$X = 6 L$	Difference	$X = 7 L$	Difference	$X = 8 L$	Difference
2°	-0.02118	0	-0.00975	0	0.02896	0
4°	-0.01922	9.25%	-0.00857	12.33%	0.02757	4.80%
6°	-0.01725	18.55%	-0.00715	27.17%	0.02616	9.67%
8°	-0.0153	27.76%	-0.00594	39.81%	0.02481	14.33%
10°	-0.01304	38.43%	-0.00437	56.22%	0.02339	19.23%
12°	-0.01163	45.09%	-0.00347	65.62%	0.02228	23.07%

The numerical values are those at the punctuation points in Figure 14. Figure 15 is a numerical diagram of wave heights at the punctuation points of the cross section. It can be seen from Figure 15 that as the drift angle increases, the amplitudes of the crests and troughs basically show a decreasing trend. The amplitude changes in the peaks and

troughs are linearly related to the drift angle changes. It can be seen that in the stratified fluid, the amplitude height of the wake generated by the variable drift angle sailing motion of the underwater vehicle is proportional to the drift angle change. The magnitude and drift angle are still clearly quantitatively related according to a linear function.

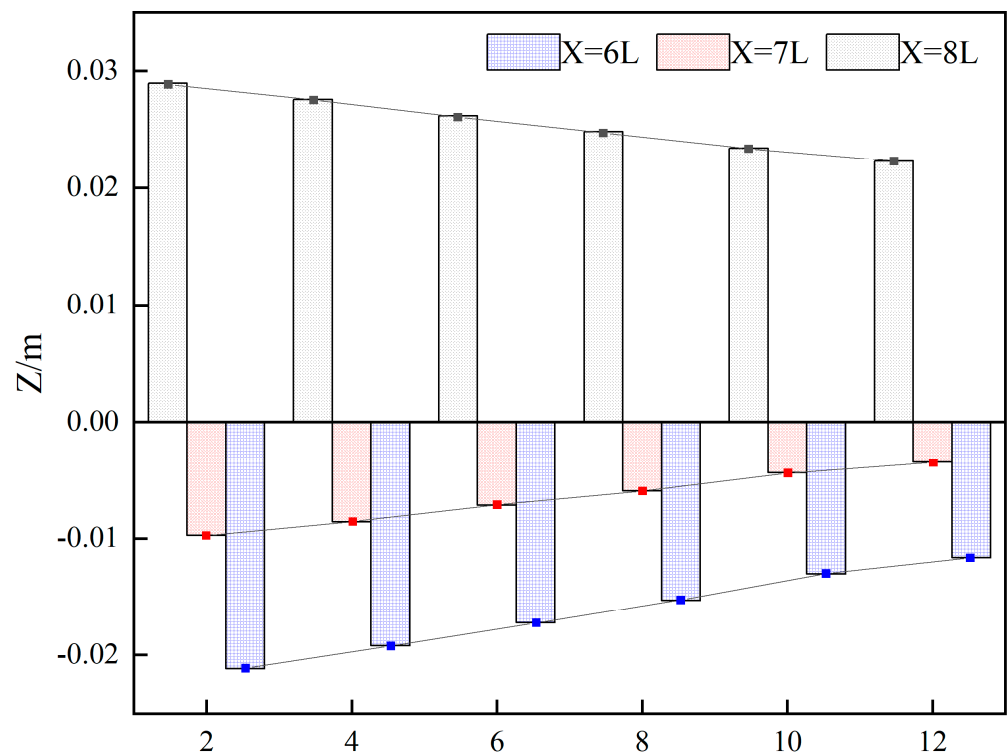


Figure 15. Wave height value at the punctuation point of the cross section.

5. Conclusions

In this paper, based on the RANS equation, the k -turbulence model and the VOF method were used to numerically simulate the variable drift angle maneuvering motion of the SUBOFF standard mode in the density layered environment. This paper focused on the analysis and research of the flow field and wake characteristics generated by the maneuvering motion of an underwater vehicle in a stratified fluid environment. The velocity flow field, side pressure, wake flow field, and characteristics around the SUBOFF were analyzed and compared under sailing conditions with variable drift angles. The influence rule of the layered environment on the hydrodynamic performance and wake characteristics of SUBOFF was intuitively determined.

First, the drag resistance was compared by numerical simulation of the towage resistance experiment of the box structure in the stratified fluid. The calculated results showed good agreement with the experimental results, indicating that the numerical method in this paper can accurately simulate the hydrodynamic performance and flow field of a SUBOFF sailing in a layered environment. Secondly, through the verification of grid independence and time step independence, a more suitable calculation model was obtained. Finally, the numerical calculation of the variable drift angle condition of SUBOFF in the layered environment was carried out. Through comparative analysis of hydrodynamic performance and wake characteristics, we studied the influence of wake characteristics caused by the maneuvering motion of SUBOFF in a layered environment.

- (1) In the stratified fluid, in the SUBOFF sailing state, the wake on the water surface exhibits a significant Kelvin wave system regardless of whether the drift angle changes; Under the simulated conditions, the change of drift angle will not cause a change in the free-surface wake wavelength, and the influence on the wake amplitude is obvious;

- (2) The greater the pressure on the SUBOFF hull part, the smaller the velocity of the flow field around this part and the more severe the fluctuation of the flow field. At the same time, causing significant changes in hydrodynamic performance and wake flow field, the asymmetry of the surrounding flow field will be strengthened with the increase in drift angle. This effect can result in significantly increased exposure of the vehicle during maneuvering motions.
- (3) Following movement of an underwater vehicle with variable drift angles, the pressure change at the maximum pressure difference between the two sides is a linear function, and the sum of the pressure reduction and increase on the left and right sides is equal. The sum of the pressure differences of different drift angles is a fixed value.
- (4) In stratified fluids, the wake varies with the drift angle and is linearly related to the amplitudes of the peaks and troughs. As the wake propagates backwards, the amplitudes at the same position at different drift angles show an obvious quantitative linear relationship.

Based on the above conclusions, the maneuvering motion of the vehicle in stratified fluid will strengthen the wave-making wake characteristics, which is not conducive to concealment of the vehicle. Therefore, in order to ensure the high concealment performance of the vehicle, it is suggested that the safety of vehicle underwater navigation be enhanced by controlling the amplitude of the vehicle's maneuvering motion. The results in this paper provide some suggestions for the selection of an appropriate navigation scheme for controlling the maneuvering motion wake of an underwater vehicle in layered fluids. They also serve as a reference for non-acoustic detection of the motion heading of an underwater vehicle under actual sea conditions and the motion trajectory of anti-reconnaissance underwater vehicles.

Author Contributions: Writing, C.S., X.C. and Z.L.; Study Design, C.S., K.H., P.L. and L.J. All authors have read and agreed to the published version of the manuscript.

Funding: This research was funded by the National Natural Science Foundation of China [grant numbers 551720105011, 51979211, 52271327, 52271330], Key Research and Development Plan of Hubei Province (2021BID008), 111 Project (BP0820028).

Institutional Review Board Statement: Not applicable.

Informed Consent Statement: Not applicable.

Data Availability Statement: The data presented in the study are available in this article (Tables and Figures).

Conflicts of Interest: The authors declare no conflict of interest.

References

1. Fang, X. *Fundamentals of Oceanic Internal Waves and China Sea Internal Waves*; Ocean University of China Press: Qingdao, China, 2005; pp. 1–4, 65–70.
2. Ekman, V.W. On dead water: The Norwegian north polar expedition 1893–1896. *Sci. Results* **1904**.
3. Osborne, A.R. Internal solitons in the Andaman sea. *Science* **1980**, *208*, 451–460. [\[CrossRef\]](#)
4. Allen, H. Schooley a1 and R. W. Stewart a2. Experiments with a self-propelled body submerged in a fluid with a vertical density gradient. *J. Fluid Mech.* **1963**, *15*, 83–96.
5. Hopfinger, E.; Flor, J.-B.; Chomaz, J.-M.; Bonneton, P. Internal waves generated by a moving sphere and its wake in a stratified fluid. *Exp. Fluids* **1991**, *11*, 255–261. [\[CrossRef\]](#)
6. Chomaz, J.M.; Bonneton, P.; Hopfinger, E.J. The structure of the near wake of a sphere moving horizontally in a stratified fluid. *J. Fluid Mech.* **1993**, *254*, 1–21. [\[CrossRef\]](#)
7. Ma, H.; Ma, B.; Zhang, R. Theoretical and experimental research on object motion wake in stratified fluid. *J. Univ. Sci. Technol. China* **2000**, *30*, 677–684.
8. Jin, J.; Liu, Z. Numerical simulation of underwater motion wake of three-dimensional spheres in stratified fluids. *China Water Transp. (Theor. Ed.)* **2006**, *4*, 83–84.
9. Jin, J. Numerical Research on Wave-Emergence Characteristics of Moving Latent Bodies in Stratified Fluids. Master's Thesis, Wuhan University of Technology, Hubei, China, 2007.

10. Chang, Y.; Zhang, J.; Hong, F. Numerical preliminary study on the wake of underwater vehicles in stratified fluids. In Proceedings of the 20th National Hydrodynamics Symposium, Fukuoka, Japan, 8–13 July 2006; pp. 665–677.
11. Brucker, K.A.; Sarkar, S. A comparative study of self-propelled and towed wakes in a stratified fluid(Article). *J. Fluid Mech.* **2010**, *652*, 373–404. [[CrossRef](#)]
12. Rottman, J.W.; Dommermuth, D.G.; Innis, G.E.; O’Shea, T.T.; Novikov, E. Numerical Simulation of Wakes in a Weakly Stratified Fluid. *arXiv* **2014**, arXiv:1410.1946.
13. Bidokhti, A.A.; Bidokhti, A. Flow Visualization of Internal Waves and Wakes of a Streamlined Body in a Stratified Fluid. *J. Appl. Fluid Mech.* **2016**, *9*, 635–641. [[CrossRef](#)]
14. Moody, Z.E.; Merriam, C.J.; Radko, T.; Joseph, J. On the structure and dynamics of stratified wakes generated by submerged propagating objects. *J. Oper. Oceanogr.* **2017**, *10*, 191–204. [[CrossRef](#)]
15. Qingjie, M.; Liang, P.; Haihua, D. Numerical prediction of suboff wake characteristics based on RANS. *Ship Sci. Technol.* **2018**, *40*, 6–11.
16. Ma, W.; Li, Y.; Ding, Y.; Duan, F.; Hu, K. Numerical investigation of internal wave and free surface wave induced by the DARPA Suboff moving in a strongly stratified fluid. *Ships Offshore Struct.* **2019**, *15*, 587. [[CrossRef](#)]
17. Ma, W.; Li, Y.; Ding, Y. Numerical simulation method of stable stratified flow and research on characteristics of flow around a sphere. *Ship Mech.* **2020**, *24*, 1278–1287.
18. Lu, W. Research on Submarine Navigation Resistance and Wave-Making Characteristics in Stratified Ocean Environment. Master’s Thesis, Dalian University of Technology, Dalian, China, 2020.
19. Zhang, Q.; Gou, Y.; Sun, J. Numerical study on the resistance characteristics of structural “dead water” in two-layer fluids. In Proceedings of the 19th China Ocean (Shore) Engineering Symposium, Chongqing, China, 11–13 October 2019.
20. Zhang, Q. *Numerical Study on the Resistance Characteristics of Two-Layer Fluid “Dead Water”*; Dalian University of Technology: Liaoning, China, 2019.
21. Wu, J.; Yu, H.; Wang, Y.; Meng, Q.; Peng, L.; Zheng, J. Numerical Simulation of Suboff Excited Free-Surface Wake in Continuous Layered Environment. *Ship Sci. Technol.* **2021**, *43*, 20–26.
22. He, G.; Liu, S.; Wang, W.; Pan, Y. Analysis of the Influence of Density Stratification on the Wave-making Resistance of Submarines Underwater Navigation. *J. Harbin Eng. Univ.* **2021**, *42*, 1125–1132.
23. Liu, S.; He, G.; Wang, W.; Gao, Y. Wake analysis of shallow navigation craft in density stratified flow. *J. Harbin Inst. Technol.* **2021**, *53*, 52–59.
24. Liu, S.; He, G.; Wang, W.; Pan, Y. Analysis of the influence of wave-making resistance of submarines sailing in deep water density layer. *J. Harbin Eng. Univ.* **2021**, *42*, 1373–1379.
25. He, G.; Liu, S.; Zhang, Z.; Zhang, W.; Wang, W.; Gao, Y.; Pan, Y. Analysis of Wave Wake of Submarine Navigating in Deep Water Density Layer. *J. Harbin Inst. Technol.* **2022**, *54*, 40–48.
26. Liu, S.; He, G.; Wang, Z.; Luan, Z.; Zhang, Z.; Wang, W.; Gao, Y. Resistance and flow field of a submarine in a density stratified fluid(Article). *Ocean. Eng.* **2020**, *217*, 107934. [[CrossRef](#)]
27. Cao, L.; Huang, F.; Wan, D.; Gao, Y. Computational Analysis of Sphere Wakes in a Linearly Stratified Fluid. *Int. J. Offshore Polar Eng.* **2021**, *31*, 309–315. [[CrossRef](#)]
28. Cao, L.-S.; Huang, F.-L.; Liu, C.; Wan, D.C. Vortical structures and wakes of a sphere in homogeneous and density stratified fluid. *J. Hydodyn. B* **2021**, *33*, 207–215. [[CrossRef](#)]
29. Huang, F.; Meng, Q.; Cao, L. Wakes and free surface signatures of a generic submarine in the homogeneous and linearly stratified fluid. *Ocean. Eng.* **2022**, *250*, 111062. [[CrossRef](#)]
30. Roddy, R.F. *Investigation of the Stability and Control Characteristics of Several Configurations of the DARPA SUBOFF Model (DTRC Model 5470) from Captive-Model Experiments*; David Taylor Research Center Bethesda Md Ship Hydromechanics Dept: Belhesda, MD, USA, 1990.